Magnesium Technology 2011
Edited by: Wim H. Sillekens, Sean R. Agnew, Neale R. Neelameggham, and Suveen N. Mathaudhu
TMS (The Minerals, Metals & Materials Society), 2011

COMPRESSIVE STRENGTH AND HOT DEFORMATION BEHAVIOR OF TX32 MAGNESIUM ALLOY WITH 0.4% Al AND 0.4% Si ADDITIONS

K.P. Rao[1], Y.V.R.K. Prasad[2], K. Suresh[1], C. Dharmendra[1], N. Hort[3], K.U. Kainer[3]

[1]Department of Manufacturing Engineering and Engineering Management
City University of Hong Kong, 83 Tat Chee Avenue Kowloon, Hong Kong SAR, China
[2]Processingmaps.com (formerly at City University of Hong Kong)
[3]GKSS Research Centre Geesthacht GmbH, Max-Planck Str. 1, Geesthact 21502, Germany

Keywords: Mg-Sn-Ca-Al-Si Alloy, Compressive Strength, Hot Workability, Processing Maps, Kinetic Analysis

Abstract

Mg-3Sn-2Ca (TX32) alloy has good corrosion and creep resistance although its strength is inferior to AZ31 alloy. In this paper, the influence of additions of 0.4%Al and 0.4%Si on the compressive strength and hot working characteristics of TX32 is reported. Although the room temperature compressive strength improved marginally with the alloying additions, the drop in higher-temperature strength is significant. By comparing with the alloy having only 0.4% Al, it is clear that the Si addition is responsible for this deterioration. The hot working behavior as characterized by processing maps revealed that TX32 exhibits two domains of dynamic recrystallization occurring in the temperature and strain rate ranges: (1) 300 – 350 °C and 0.0003 – 0.001 s^{-1} and (2) 390 – 500 °C and 0.005 – 0.6 s^{-1}. In Al and Si containing TX32, both the domains moved to higher temperatures and the flow instability is reduced improving the hot workability. In both the domains, the apparent activation energy is higher than that for self-diffusion in magnesium implying that there is a significant contribution from the back stress generated by the hard particles present in the matrix.

Introduction

Their light weight is the main reason that makes Mg based alloys attractive for components in aerospace and automobile applications. However, many of the wrought alloys like Mg-3Al-1Zn have inferior corrosion and creep properties and to improve these two properties newer Mg-Sn-Ca alloys (TX series) are being developed [1-3]. In this system, Sn forms a solid solution with Mg and imparts corrosion resistance while Ca enhances high temperature creep strength by forming CaMgSn intermetallic particles. The first and foremost alloy in this system is Mg-3Sn-1Ca (TX31), which was characterized as regards its corrosion resistance and processability [4-6]. The creep resistance of this alloys can be further improved by increasing the Ca content to 2% but with a small compromise of corrosion properties [3,7]. In the microstructure of Mg-3Sn-2Ca [3], intermetallic particles of CaMgSn form mostly in the matrix and Mg_2Ca phase forms at the grain boundaries both of which are beneficial in enhancing the creep strength. However, there is a need to strengthen the alloy further to make it a candidate material for structural applications. For this purpose, alloying with aluminum and silicon is considered to be attractive since Al causes solid solution strengthening of Mg as there is a significant difference in the atomic diameters of Mg and Al, while Si forms intermetallic particles that can enhance the creep strength. With this in view, Mg-3Sn-2Ca-0.4Al-0.4Si alloy has been designed and chosen for this investigation. The aim of the present investigation is to evaluate the compressive strength and hot working characteristics of this alloy with a view to understand the effect of the combined additions of Al and Si to TX32. For this purpose, the compressive strength of Mg-3Sn-2Ca-0.4Al-0.4Si is measured in the temperature range 25 – 250 °C and the hot working behavior is evaluated in the temperature range 300 – 500 °C. It is proposed to compare the behavior of this alloy with those of Mg-3Sn-2Ca and Mg-3Sn-2Ca-0.4Al.

The hot working behavior has been characterized with the help of the standard kinetic approach [8] as well as processing maps [9,10]. The standard kinetic rate equation relating the steady state flow stress (σ) to strain rate ($\dot{\varepsilon}$) and temperature (T) is given by [8]:

$$\dot{\varepsilon} = A\sigma^n \exp\left[-\frac{Q}{RT}\right] \quad (1)$$

where A = constant, n = stress exponent, Q = activation energy, and R = gas constant. The rate-controlling mechanisms are identified on the basis of the activation parameters n and Q.

Processing maps are based on the Dynamic Materials Model [11], the principles of which were described in earlier publications [9,12]. Briefly, the work-piece undergoing hot deformation is considered to be a dissipator of power and the strain rate sensitivity (m) of flow stress is the factor that partitions power between deformation heat and microstructural changes. The efficiency of power dissipation occurring through microstructural changes during deformation is derived by comparing the non-linear power dissipation occurring instantaneously in the work-piece with that of a linear dissipater for which the m value is unity, and is given by:

$$\eta = 2m/(m+1) \quad (2)$$

The variation of efficiency of power dissipation with temperature and strain rate represents a *power dissipation map* which is generally viewed as an iso-efficiency contour map. Further, the extremum principles of irreversible thermodynamics as applied to continuum mechanics of large plastic flow [13] are explored to define a criterion for the onset of flow instability given by the equation for the instability parameter $\xi(\dot{\varepsilon})$:

$$\xi(\dot{\varepsilon}) = \frac{\partial \ln[m/(m+1]}{\partial \ln \dot{\varepsilon}} + m \leq 0 \quad (3)$$

The variation of the instability parameter as a function of temperature and strain rate represents an *instability map* which delineates regimes of instability where $\xi(\dot{\varepsilon})$ is negative. A superimposition of the instability map on the power dissipation map gives a *processing map* which reveals *domains* (efficiency contours converging towards a peak efficiency) where individual

microstructural processes occur and the limiting conditions for the *regimes* (bounded by a contour for $\xi(\dot{\varepsilon}) = 0$) of flow instability. Processing maps help in identifying temperature – strain rate windows for hot working where the intrinsic workability of the material is maximum (e.g. dynamic recrystallization (DRX) or superplasticity) and also in avoiding the regimes of flow instabilities (e.g. adiabatic shear bands or flow localization).

Experimental

Mg – 3 wt.% Sn – 2 wt.% Ca – 0.4 wt.% Al – 0.4 wt.% Si alloy was prepared using 99.99% pure Mg, 99.96% pure Sn, 98.5% pure Ca, 99.9% Al and 99.9% Si. The alloy, molten at about 720 °C, was kept under a protective cover of Ar+3% SF_6 gas before casting in a pre-heated permanent mold to obtain cylindrical billets of 100 mm diameter and 350 mm length.

Cylindrical specimens of 10 mm diameter and 15 mm height were machined from the as-cast billet for compression testing. For inserting a thermocouple to measure the specimen temperature as well as the adiabatic temperature rise during deformation, the specimens were provided with a 1 mm diameter hole machined at mid height to reach the centre of the specimen.

For the purpose of evaluating the compressive strength of the alloy, compression tests were conducted at a strain rate of 0.0001 s^{-1} and in the temperature range 25–250 °C using a computer-controlled servo-hydraulic testing machine. The data for developing processing maps were obtained in isothermal uniaxial compression tests were conducted at constant true strain rates in the range 0.0003 – 10 s^{-1} and temperature range 300 – 500 °C. Details of the test set-up and procedure are described in earlier publication [14]. Constant true strain rates during the tests were achieved using an exponential decay of actuator speed in the servo hydraulic machine. Graphite powder mixed with grease was used as the lubricant in all the experiments. The specimens were deformed up to a true strain of about 1.0 and then quenched in water. The load – stroke data were converted into true stress – true strain curves using standard equations. The flow stress values were corrected for the adiabatic temperature rise at different temperatures and strain rates and this correction was less important at lower strain rates and higher temperatures. The deformed specimens were sectioned in the center parallel to the compression axis and the cut surface was mounted, polished and etched for metallographic examination. All the specimens were etched with an aqueous solution containing 3% picric acid.

Results and Discussion

The microstructure of the starting material in cast condition is dendritic and consisted of very large grains (about 500 μm diameter). While the CaMgSn particles are present both in the matrix and at the grain boundaries, Mg_2Ca phase is essentially present at the grain boundaries. Other intermetallics phases including Mg_2Si are also present in the microstructure.

High Temperature Strength

The variation of the ultimate compressive strength of Mg-3Sn-2Ca-0.4Al-0.4Si alloy with temperature in the range 25 – 250 °C obtained at a strain rate of 0.0001 s^{-1} is shown in Figure 1. A strain rate slower than those used for generating processing maps is selected for obtaining the strength values since the material does not have much ductility in this temperature range [15]. The strength drops fast with temperature and reaches a near plateau beyond about 150 °C up to 200 °C beyond which it drops precipitously. The values for the base alloy Mg-3Sn-2Ca and the one with 0.4%Al addition are also included in this figure for the purpose of comparison and to evaluate the effects of additions of Al alone and of Al+Si. The alloy with only 0.4 wt% Al has shown increased strength compared to their TX32 base (Al free alloy) at almost all the test temperatures. Aluminum improves room temperature mechanical properties of Mg by solid solution strengthening due to large atomic size difference (α-Mg) and also precipitation of (β-$Mg_{17}Al_{12}$) intermetallic phase [16]. However, with the addition of 0.4% Si to this alloy decreases the higher temperature strength much more significantly between 100 and 200 °C. This reduction is likely due to the formation of Mg_2Si particles. It is the only stable compound that forms in the Mg-Si System. The Si addition often promotes the precipitation of Mg_2Si particles which form during solidification and are quite detrimental to the mechanical properties of Mg alloys [17,18]. It is reported [19] that the addition of Si to AZ91 alloy does not change the quantity as well as the morphology of the $Mg_{17}Al_{12}$ phase. It may be due to negligible solid solubility of Si in Mg and the impossibility of the formation of any other compound containing Al and Si. On the other hand, Nanjunda Swamy et al. [20] observed that, in cast Mg-Al-Si composites, ultimate tensile strength (UTS) decreases with increasing Mg_2Si content possibly due to increased casting defects such as porosity and segregation which may be counteracting the strengthening effect of increasing Mg_2Si content. Asl et al. [16] have indicated that addition of Si to some aluminum containing magnesium alloys improves creep resistance while reducing the room temperature mechanical properties. With such differing observations, the role of Si on mechanical and creep properties of such alloy systems is not fully understood. The present results clearly show that unlike the Al addition, Si addition to the extent of 0.4% is not useful for improving the strength property of the base alloy.

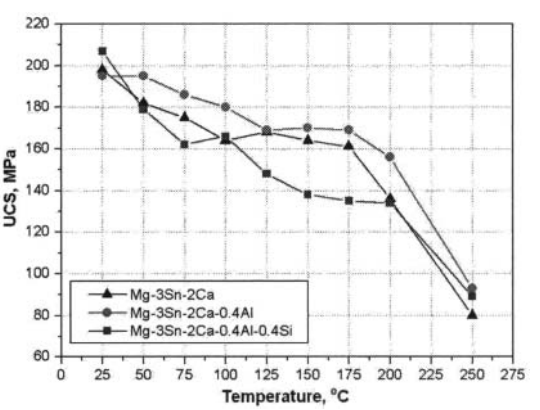

Figure 1. Variation of ultimate compressive strength (UCS) of as-cast Mg-3Sn-2Ca, Mg-3Sn-2Ca-0.4Al, and Mg-3Sn-2Ca-0.4Al-0.4Si alloys with temperature.

Hot Working Behavior

The processing map obtained at a strain of 0.5 (near steady-state flow) covering a temperature range 300 – 500 °C and strain rate range 0.0003 – 10 s^{-1} for the alloy Mg-3Sn-2Ca-0.4Al-0.4Si is shown in Figure 2. The map exhibits two domains occurring in the temperature and strain rate ranges given as follows:

Domain #1: 300 – 410 °C and 0.0003 – 0.003 s^{-1} with a peak efficiency of 38% occurring at 350 °C and 0.0003 s^{-1}.
Domain #2: 420 °C – 500 °C and 0.003 – 3 s^{-1} with a peak efficiency of 39% occurring at 500 °C and 0.1 s^{-1}.
In addition, two flow instability regimes occur: (1) at temperatures lower than 360°C and strain rates higher than 0.01 s^{-1}, (2) at higher temperatures 430 – 490 °C and strain rate of 10 s^{-1}. The second regime covers only a small region and may be ignored.

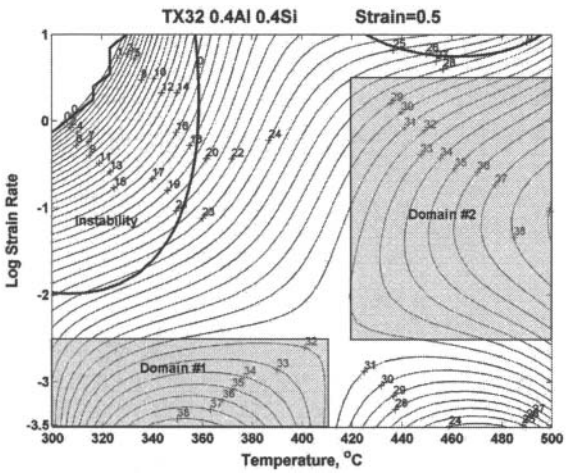

Figure 2. Processing map for Mg-3Sn-2Ca-0.4Al-0.4Si alloy. The numbers against the contours represent efficiency of power dissipation in percent. The dark line separates the flow instability regimes. The blank region at left hand top corner represents cracking of the specimens.

The microstructures recorded at 350 °C/0.0003 s^{-1} (Domain #1) and at 500 °C/0.1 s^{-1} (Domain #2), are shown in Figure 3 (a) and (b). Both these microstructures indicate that the as-cast microstructure is converted into an equiaxed wrought microstructure through a mechanism involving dynamic recrystallization (DRX). It is interesting to note that there are two DRX domains separated at about 410 °C. In terms of dissipative energy which will be low when the efficiency of power dissipation is high, this change-over region may be viewed as a saddle point configuration [12]. It is possible that such a configuration has formed due to the difference in the operating slip systems. Below 400 °C, the flow is dominated by prismatic slip and basal slip, in which case the recovery mechanism is going to be climb of edge dislocations. In this case, cross-slip is ruled out since the stacking fault energy on basal slip systems is lower [21]. It is well known that at temperatures higher than 400 °C, the pyramidal slip systems dominate the flow and the recovery mechanism will be cross-slip since the stacking fault energy on the pyramidal slip systems will be high [22]. Processing at temperatures close to the saddle point is not desirable since it may lead to microstructural instability.

Using the standard kinetic rate equation (Eq. 1) to represent the steady-state flow under hot working conditions [8], the activation parameters – stress exponent (n) and apparent activation energy (Q) – are evaluated. A plot of log(flow stress) versus log(strain rate) at different test temperatures, is shown in Figure 4. All the data at the temperature of 500 °C (Domain #2) exhibited a good linear fit with a slope (m) of 0.225 or stress exponent (n) of 4.44. With decreasing temperatures, the linear fit got progressively limited to lower strain rates (Domain #1) and the m value is 0.2 or stress exponent (n) is 5.0. At higher strain rates and lower temperatures, where the rate equation (Eq. 1) is not obeyed, flow instability occurs.

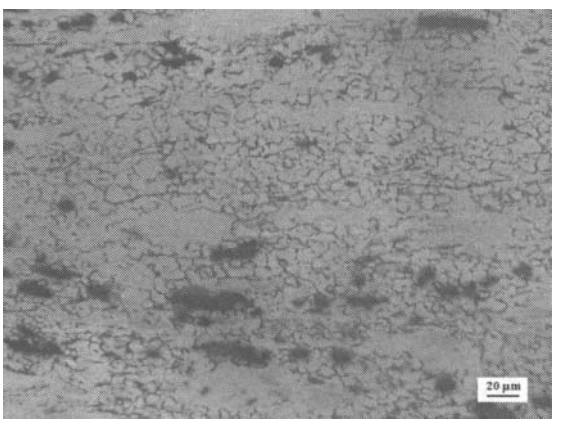

Figure 3(a). Microstructure of Mg-3Sn-2Ca-0.4Al-0.4Si alloy deformed at 350 °C and 0.0003 s^{-1} (Domain #1) exhibiting dynamic recrystallization of as-cast microstructure.

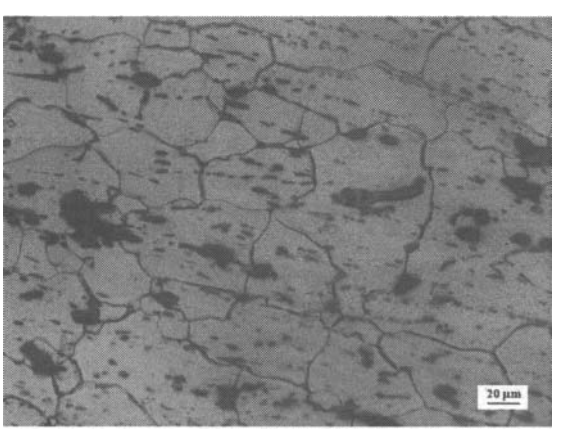

Figure 3(b). Microstructure of Mg-3Sn-2Ca-0.4Al-0.4Si alloy deformed at 500 °C and 0.1 s^{-1} (Domain #2) exhibiting dynamic recrystallization of as-cast microstructure.

Arrhenius plot relating normalized flow stress [ln (σ/μ)] to ($1/T$) (μ = shear modulus of Mg) is shown in Figure 5. The data at strain rates of 0.0003 s^{-1} and 0.001 s^{-1} exhibited a linear fit giving an apparent activation energy of 177 kJ/mole. On the other hand, the data at strain rates of 0.01 s^{-1} to 1 s^{-1} gave a linear fit progressively at higher temperatures and also yielded an apparent activation energy of 177 kJ/mole.

The apparent activation energy values obtained in the two different regimes are larger than that for lattice self diffusion in Mg (135 kJ/mole) [23]. This could be due to the large back stress generated by the large volume fraction of CaMgSn intermetallic particles in the matrix.

For hot working, dynamic recrystallization (DRX) domain is preferred since it helps in converting the as-cast dendritic microstructure by an equi-axed wrought microstructure. While processing in the lower strain rate domain (Domain #1) is too

slow from industrial view point, hot working in Domain #2 is recommended for this alloy, the optimum parameters being 500 °C/0.1 s^{-1}. However the hot working window is wide suggesting that this alloy is highly workable.

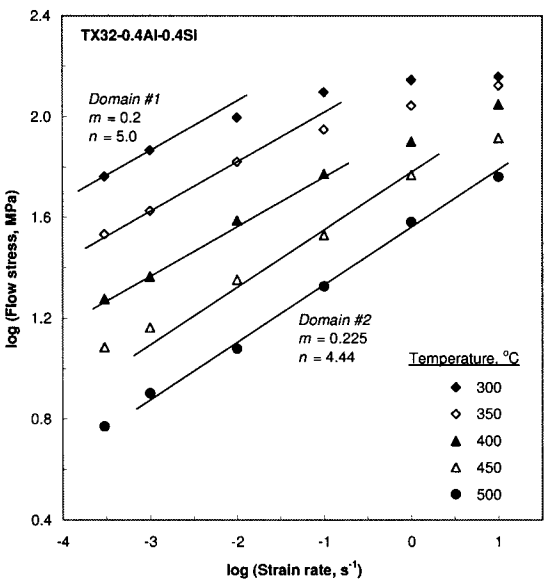

Figure 4. Variation of flow stress (at a strain of 0.5) of Mg-3Sn-2Ca-0.4Al-0.4Si alloy with strain rate on a log-log scale at different test temperatures.

Comparison with Mg-3Sn-2Ca and Mg-3Sn-2Ca-0.4Al Alloys

The processing maps for the base alloy Mg-3Sn-2Ca is shown in Figure 6, which also exhibits two domains of dynamic recrystallization in the temperature and strain rate ranges given as follows: (1) 300 – 350 °C and 0.0003 – 0.001 s^{-1} with a peak efficiency of 42% occurring at 300 °C and 0.0003 s^{-1}, and (2) 390 – 500 °C and 0.005 – 0.6 s^{-1} with a peak efficiency of 42% occurring at about 450 °C and 0.03 s^{-1}. A comparison of the two processing maps (Figures 2 and 6) reveals that both the DRX domains have shifted to higher temperatures by the addition of Al and Si. Domain #1 has expanded from 350 °C to 410 °C and Domain #2 has commenced at a higher temperature of 420 °C by the addition of Al and Si compared to 390 °C for the base TX32 alloy. Also, the strain rate range for domain #1 has slightly increased whereas that for domain #2 is significantly broadened with a range of 0.003 - 3 s^{-1} compared to 0.005 - 0.6 s^{-1} for TX32 alloy. In addition, the flow instability regime is reduced with the addition of Al and Si. Both these changes are favorable for the hot workability since the workability windows are expanded by these two additions. This effect is essentially due to increased volume fraction of intermetallic particles due to the formation of Mg_2Si in the Si containing alloy. Higher temperatures are required to overcome the back stress before the recovery processes including climb or cross-slip to occur. Another noteworthy feature is that the saddle point configuration has not changed by the addition of Al and Si. This is in support of the earlier interpretation in terms of the change in the dominant slip mechanisms from basal+prismatic slip to pyramidal slip, which is not influenced by minor alloying additions. The reduced flow instability at higher temperatures may be interpreted in terms of the promotion of cross-slip by the Mg_2Si particles in addition to CaMgSn particles.

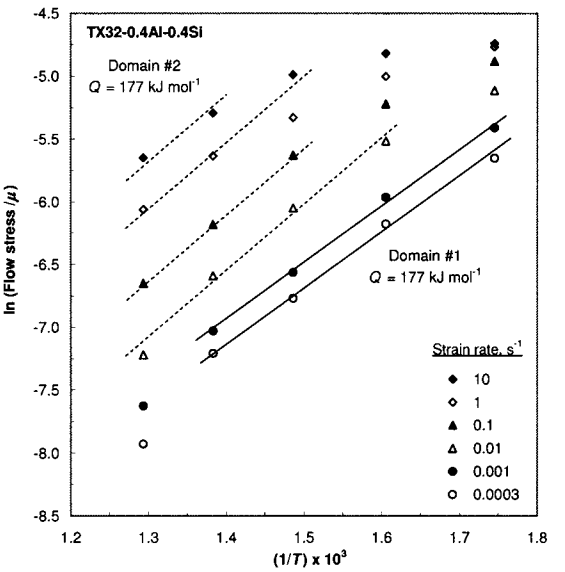

Figure 5. Arrhenius plot showing the variation of normalized flow stress of Mg-3Sn-2Ca-0.4Al-0.4Si with inverse of temperature at different strain rates.

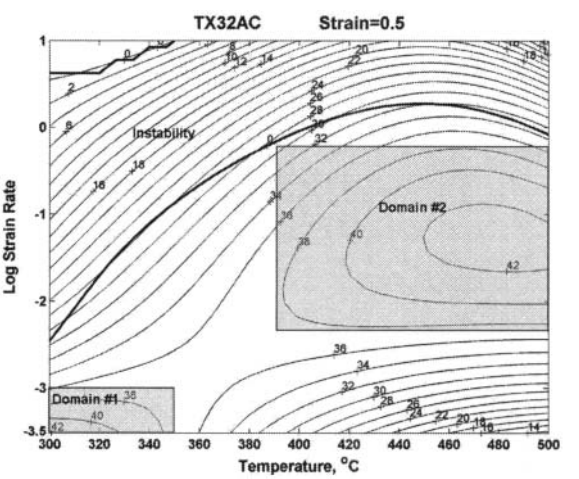

Figure 6. Processing map for Mg-3Sn-2Ca as-cast alloy. The numbers against the contours represent efficiency of power dissipation in percent. The dark line separates the flow instability regimes. The blank region at left hand top corner represents cracking of the specimens.

The activation parameters evaluated in the two domains of all the alloys are shown in Table 1. The values are nearly unchanged due to Al additions [24] while the activation energy value for Domain #2 decreased due to Si addition. This further supports the interpretation that Mg_2Si particles promote the recovery by cross-slip in this domain by increasing the barriers to dislocation movement. However, the kinetics of the climb process controlling Domain #1 is not much influenced by these particles.

Table 1. Activation parameters for Mg-3Sn-2Ca, Mg-3Sn-2Ca-0.4Al, and Mg-3Sn-2Ca-0.4Al-0.4Si alloys

Alloy (as-cast)	Domain #1		Domain #2	
	n	*Q* kJ/mole	*n*	*Q* kJ/mole
Mg-3Sn-2Ca	4.54	177	4.54	197
Mg-3Sn-2Ca-0.4Al	4.54	175	4.54	195
Mg-3Sn-2Ca-0.4Al-0.4Si	5.0	177	4.44	177

Summary and Conclusions

The compressive strength of Mg-3Sn-2Ca-0.4Al-0.4Si alloy in as-cast condition has been evaluated in the temperature range 25 – 250°C and compared with that of the base alloy Mg-3Sn-2Ca and Mg-3Sn-2Ca-0.4Al alloy with a view to assess the effect of Al and Si additions. The hot deformation behavior has also been studied using hot compression tests in the temperature range 300 – 500 °C and strain rate range 0.0003 – 10 s^{-1}. The flow stress data have been analyzed using processing maps and standard kinetic analysis. The effect of Al and Si additions to the hot working behavior has also been assessed by comparing the behaviors. The following conclusions are drawn from this investigation.

(1) The compressive strength of Mg-3Sn-2Ca alloy has increased due to the addition of 0.4 Al but deteriorated by the Si addition, particularly at higher temperatures.

(2) The deterioration in strength may have been caused by the formation of Mg_2Si particles, although the exact reason is unclear.

(3) The processing map for Mg-3Sn-2Ca-0.4Al-0.4Si alloy exhibited two domains in the temperature and strain rate ranges given by: (1) 300 – 410 °C and 0.0003 – 0.003 s^{-1} with a peak efficiency of 38% occurring at 350 °C and 0.0003 s^{-1} and (2) 420 °C – 500°C and 0.003 – 3 s^{-1} with a peak efficiency of 39% occurring at 500 °C and 0.1 s^{-1}.

(4) Comparison of processing map of Mg-3Sn-2Ca-0.4Al-0.4Si with that of the base alloy (Mg-3Sn-2Ca) revealed that both the domains have moved to higher temperatures and the flow instability regime reduced particularly at higher temperatures due to the addition of Al and Si. The basic features however remained unchanged.

(5) Both the domains represent the process of dynamic recrystallization. It is suggested that the rate controlling mechanism in the lower strain rate domain is climb while it is cross-slip in the higher temperature domain.

(6) The apparent activation energy obtained by kinetic analysis in both the domains of the map for Mg-3Sn-2Ca-0.4Al-0.4Si is 177 kJ/mole, which is higher than that for self diffusion in Mg.

(7) The apparent activation energy in the lower strain rate domain is similar to that obtained for the base alloy while it is lower in the second domain, suggesting that cross-slip is promoted by Mg_2Si particles.

(8) The addition of Si is favorable for enhancing the hot workability since it widens the processing window.

Acknowledgement

This work was supported by a grant (Project #115108) from the Research Grants Council of the Hong Kong Special Administrative Region, China.

References

1. T. Abu Leil et al., "Corrosion Behavior and Microstructure of a Broad Range of Mg-Sn-X Alloys," *Magnesium Technology 2006*, ed. A.A. Luo, N.R. Neelameggham and R.S. Beals (Warrendale, PA: The Minerals, Metals and Materials Society, 2006), 281-286.

2. T. Abu Leil et al., "Effect of Heat Treatment on the Microstructure and Creep Behavior of Mg-Sn-Ca Alloys," *Mater. Sci. Forum*, 546-549 (2007), 69-72.

3. T. Abu Leil et al., "Microstructure, Corrosion and Creep of As-cast Magnesium Alloys Mg-2Sn-2Ca and Mg-4Sn-2Ca," *Magnesium Technology 2007*, ed. R.S. Beals, A.A. Luo, N.R. Neelameggham, and M.O. Pekguleryuz (Warrendale, PA: The Minerals, Metals and Materials Society, 2007), 257-262.

4. Y.V.R.K. Prasad et al., "Hot Working Parameters and Mechanisms in As-Cast Mg-3Sn-1Ca Alloy," *Mater. Letters*, 62 (2008), 4207-4209.

5. Y.V.R.K. Prasad et al., "Hot Workability Characteristics of Cast and Homogenized Mg-3Sn-1Ca Alloy," *Jour. Mater. Proc. Tech.*, 201 (2008), 359-363.

6. Y.V.R.K. Prasad et al., "Optimum Parameters and Rate-Controlling Mechanisms for Hot Working as Extruded Mg-3Sn-1Ca Alloy," *Mater. Sci. Eng., A* 502 (2009), 25-31.

7. N. Hort et al., "Creep and Hot Working Behavior of a New Magnesium Alloy Mg-3Sn-2Ca," *Magnesium Technology 2008*, ed. M.O. Pekguleryuz, N.R. Neelameggham, R.S. Beals, and E.A. Nyberg (Warrendale, PA: The Minerals, Metals and Materials Society, 2008), 401-406.

8. J.J. Jonas, C.M. Sellars, and W.J. McG. Tegart, "Strength and Structure under Hot-Working Conditions," *Metall. Rev.*, 14 (1969), 1-24.

9. Y.V.R.K. Prasad and T. Seshacharyulu, "Modeling of Hot Deformation for Microstructural Control," *Inter. Mater. Rev.*, 43 (1998), 243-258.

10. Y.V.R.K. Prasad and S. Sasidhara, *Hot Working Guide: A Compendium of Processing Maps* (Materials Park OH: ASM International, 1997).

11. Y.V.R.K. Prasad et al., "Modeling of Dynamic Material Behavior in Hot Deformation: Forging of Ti-6242," *Metall. Trans.*, 15A (1984), 1883-1892.

12. Y.V.R.K. Prasad, "Processing Maps – A Status Report," *Jour. Mater. Eng. Perf.*, 12 (2003), 638-645.

13. H. Ziegler, "Some Extremum Principles in Irreversible Thermodynamics with Applications to Continuum Mechanics," *Progress in Solid Mechanics*, ed. I.N. Sneddon and R. Hill, Vol.4 (New York: Wiley, 1965), 91-193.

14. Y.V.R.K. Prasad, and K.P. Rao, "Processing Maps for Hot Deformation of Rolled AZ31 Magnesiuim Alloy Plate:

Anisotropy of Hot Workability," *Mater. Sci. Eng., A* 487 (2008), 316-327.

15. K.P. Rao et al., "Effect of Minor Additions of Al and Si on the Mechanical Properties of Cast Mg-3Sn-2Ca Alloys in Low Temperature Range," *Mater. Sci. Forum*, 654-656 (2010), 635-638.

16. K.M. Asl, A. Tari, and F. Khomamizadeh, "The Effect of Different Content of Al, RE and Si Element on the Microstructure, Mechanical and Creep Properties of Mg-Al Alloys," *Mater. Sci. Eng., A* 523 (2009), 1-6.

17. D.H. Kang, S.S. Park, and N.J. Kim, "Development of Creep Resistant Die Cast Mg-Sn-Al-Si Alloy," *Mater. Sci. Eng., A* 413-414 (2005), 555-560.

18. M.S. Dargusch et al., "The Effect of Silicon Content on the Microstructure and Creep Behavior in Die-Cast Magnesium AS Alloys," *Metall. Mater. Trans.*, 35A (2004), 1905-1909.

19. A. Srinivasan, U.T.S. Pillai, and B.C. Pai, "Microstructure and Mechanical Properties of Si and Sb Added AZ91 Magnesium Alloy," *Metall. Mater. Trans.*, 36A (2005), 2235-2243.

20. H.M. Nanjunda Swamy, S.K. Nath, and S. Ray, "Tensile and Fracture Properties of Cast and Forged Composite Synthesized by Addition of Al-Si Alloy to Magnesium," *Metall. Mater. Trans.*, 40A (2009), 3284-3293.

21. D.H. Sastry, Y.V.R.K. Prasad, and K.I. Vasu, "On the Stacking Fault Energies of Some Close-Packed Hexagonal Metals," *Scripta Metall., 3(1969)927-929.*

22. J.R. Morris et al., "Prediction of a {1122} hcp Stacking Fault Using a Modified Generalized Stacking-Fault Calculation," *Philos. Mag., A76* (1997), 1065-1077.

23. H.J. Frost, and M.F. Ashby, *Deformation-Mechanism Maps: The Plasticity and Creep of Metals and Ceramics* (Oxford: Pergamon Press, 1982), 44.

24. K.P. Rao et al., "Effect of Aluminum Addition on the Strengthening and High Temperature Deformation Behavior of Mg-3Sn-2Ca Alloy," *Magnesium Technology 2010,* ed. S.R. Agnew, N.R. Neelameggham, E.A. Nyberg, and W.H. Sillekens (Warrendale, PA: The Minerals, Metals and Materials Society, 2010) 201-205.